Journal of Membrane Science 585 (2019) 191–198

Contents lists available at ScienceDirect

Journal of Membrane Science

journal homepage: www.elsevier.com/locate/memsci

Graphene oxide nanosheet as a two-dimensional polyelectrolyte: pH-responsive behavior of a multilayered nanomembrane

Eungjin Ahn[a,1], Houda Gaiji[b,c,1], Taehyung Kim[d], Manef Abderrabba[c], Hyun-Wook Lee[d], Byeong-Su Kim[a,*]

[a] Department of Chemistry, Yonsei University, Seoul, 03722, Republic of Korea
[b] Department of Chemistry, Faculty of Mathematical, Physical and Natural Sciences of Tunis, University Tunis El Manar, Tunis, 2092, Tunisia
[c] Laboratory of Materials Molecules and Applications (LMMA), Preparatory Institute of Scientific and Technical Studies (IPEST), University of Carthage, La Marsa, Tunis, 2070, Tunisia
[d] Department of Energy Engineering, Ulsan National Institute of Science and Technology (UNIST), Ulsan, 44919, Republic of Korea

ARTICLE INFO

Keywords:
Graphene oxide
Layer-by-Layer assembly
Nanomembrane
Swelling
Ion-permselectivity

ABSTRACT

Graphene oxide (GO) is a promising two-dimensional (2D) nanomaterial that could improve the performance of membranes due to its unique mechanical stability and chemical tunability. Moreover, GO nanosheets may act as 2D polyelectrolytes in solution because the abundant surface functional groups confer them high dispersity. Unlike conventional polyelectrolyte systems, the assembly behavior of this 2D polyelectrolyte and its resulting characteristics in multilayered membranes have not been thoroughly investigated. Herein, we employed a layer-by-layer (LbL) assembly technique to assemble GO multilayered membranes with highly controlled thickness, roughness, and charge density depending on the assembly pH conditions. Compared to conventional GO membranes prepared by vacuum filtration, the LbL assembled GO multilayered membranes presented different internal structure, wettability, and ion-permeability. The unique properties of the 2D polyelectrolytes obtained in this study may broaden their potential in the field of materials science and membrane applications.

1. Introduction

Polyelectrolytes, polymeric materials with ionizable groups, are one of the most important macromolecules in materials and polymer science [1]. The combination of the physics of ionized systems and the chemistry of polymeric chains results in unique characteristics of great interest. The ionization of polyelectrolytes, for example, is highly sensitive to environmental conditions, including solvent polarity, pH, ionic strength and temperature, inducing a stimuli-responsive behavior in these molecules [2,3]. These characteristics are relevant from a scientific and technological perspective, particularly when considering the adsorption or interaction of polyelectrolytes with other molecules and surfaces. During the past decades, there has been significant progress in the application of polyelectrolytes for the design of functional materials and advanced surface modification [4–8].

Graphene, a single-layered two-dimensional (2D) carbon lattice, is a promising carbon nanomaterial with remarkable electrical, chemical, and mechanical properties [9]. As an alternative for pristine graphene, chemically exfoliated graphene oxide (GO) nanosheets are solution processable, providing interesting opportunities to develop advanced materials [10,11]. With its unique atomically thin 2D structure, GO can readily form layer-stacked films that can be used in membranes and coating applications [12–17]. Owing to the presence of rich functional groups in its surface, such as carboxylic acid and hydroxyl, GO nanosheets can be readily dispersed in polar solvents and behave as 2D polyelectrolytes. Despite the vast number of reports showing the superior properties of GO nanosheets, particularly in the field of energy materials, it is still necessary to explore its capability as a 2D polyelectrolyte, particularly for its membrane applications.

Layer-by-layer (LbL) assembly is a versatile thin film fabrication technique that offers unique and attractive opportunities to prepare nanostructured materials on various surfaces. Among the different intermolecular interactions used for LbL assembly, electrostatic interaction is the most fundamental means to assemble oppositely charged polyelectrolytes. This results in the formation of polyelectrolyte multilayers with various formats, including planar surface coating, colloid particles, and complex membranes with a controlled composition of nanoscale precision [18–20]. In combination with the unique features

* Corresponding author.
E-mail address: bskim19@yonsei.ac.kr (B.-S. Kim).
[1] These authors contributed equally.

https://doi.org/10.1016/j.memsci.2019.05.035
Received 18 December 2018; Received in revised form 8 May 2019; Accepted 14 May 2019
Available online 17 May 2019
0376-7388/

of polyelectrolytes, the properties of membranes are often governed by the assembly and post-assembly conditions, which affect the thickness, internal structure, mechanical strength, and permeability [21].

The development of graphene-based nanomaterials *via* LbL assembly not only introduces a new addition to the existing library of LbL materials but may also help to overcome some limitations in the physical and chemical properties of conventional polyelectrolytes [22–24]. Moreover, the application of GO assemblies in coatings and membranes requires a fundamental study that compares the GO assembly with conventional polyelectrolyte multilayers. The unique 2D architecture of a GO assembly, which possesses several defects and grain boundaries for the penetration of ions within densely packed interlayers, should be useful as a filtration membrane. Accordingly, Geim et al. and other research groups have proved the precise control of the permeation of water, gas, and dissolved ions through GO-based membranes [25,26]. However, these investigations have been limited to vacuum-assisted filtration of a single GO component for the preparation of the membrane [27–29].

In this work, we evaluate the properties of a GO-based membrane focusing on its swelling behavior under various conditions. Unlike previous reports, we employed a dual GO component system, *i.e.*, positively charged amine-functionalized graphene oxide (GO^+) and negatively charged graphene oxide (GO^-), for the assembly of a GO membrane *via* the LbL method. These unique 2D polyelectrolytes were assembled under various pH conditions, allowing for the fine control of important parameters, including thickness, morphology, charge density, and internal structure. This, in turn, dictates the molecular permeability through the GO nanomembrane. The properties of the 2D polyelectrolytes obtained in this study will likely improve the preparation of GO assemblies toward coatings and membranes applications.

2. Materials and methods

2.1. Fabrication of graphene oxide (GO^-) nanosheet

All chemicals were of analytical grade and used as received. All aqueous solutions were prepared using ultra-pure de-ionized (DI) water from a Milli-Q system. The reagents graphite, P_2O_5, $K_2S_2O_8$, $KMnO_4$, HCl, H_2O_2, H_2SO_4, KOH, 1-ethyl-3-(3-dimethylaminopropyl)carbodiimide (EDC), ethylenediamine and poly (ethylene imine) (PEI) were purchased from Sigma Aldrich. Graphene oxide (GO^-) was prepared from graphite powder according to the modified Hummer methods [30,31]. The detailed synthetic process is described in the Supporting Information.

2.2. Synthesis of amine-functionalized graphene oxide (GO^+)

A positively charged GO solution, GO^+, was synthesized as the counterpart of the negatively charged GO for the LbL assembly. The amine-functionalized GO^+ was prepared by attaching ethylene diamine to the carboxylic acid groups of GO^- *via* an EDC coupling reaction. The carboxylic acids in GO were replaced with amine groups, providing a positive surface charge under a wide pH range. Specifically, 1.25 g of EDC was slowly added to 100 mL of a carboxylated GO^- solution (0.50 mg/mL) under vigorous stirring. Then, 10 mL of ethylene diamine was added, and the mixture was allowed to react overnight at room temperature under constant agitation. The resulting solution was dialyzed in DI water until the pH of dialysis fluid was neutral [32].

2.3. Fabrication of the GO multilayered membrane

GO LbL films were prepared using an automated spin-assisted dipping machine (NanoStrata Inc., USA) on either a silicon wafer or quartz glass substrate. Aqueous solutions of GO^- and GO^+ were prepared (0.50 mg/mL) and used at different pH conditions. The pH was adjusted using appropriate volumes of 1.0 M HCl or NaOH. Prior to use, the silicon and quartz substrates were carefully cleaned with a piranha solution (7:3 v/v mixture of 98% H_2SO_4 and 32% H_2O_2) at 120 °C for 1 h, then thoroughly rinsed with pure water and dried with a gentle nitrogen stream. Finally, the substrates were subjected to a 10-min plasma treatment to induce a negative surface charge. Therefore, the first step in the LbL assembly was the adsorption of GO^+ on the substrate. Each step consisted of a 10-min dipping followed by three times washing in pH-adjusted DI water for 1 min each. The process was then repeated until reaching the desired number of bilayers in the $(GO^+/GO^-)_n$ multilayered membrane.

2.4. Characterization of GO nanomembranes

ζ-potential was measured using a Zetasizer (Malvern Instruments Ltd.). FT-IR (Varian, 670-IR) spectroscopy was used to determine the chemical structure of the GO sheets. The UV–vis absorbance spectra of the GO multilayer film on quartz were recorded using a Cary 5000 UV–vis spectroscopy (Varian). The thickness of both the dry and wet $(GO^+/GO^-)_n$ multilayers was characterized *via* ellipsometry (J. A. Woollam Co., Alpha-SE) from 380 to 900 nm with a B-spline film modeling. The surface morphology of the prepared GO sheets and the surface roughness of the GO multilayer films were analyzed using atomic force microscopy (AFM, Veeco Instruments Inc., DI-3100) and field-emission scanning electron microscopy (FE-SEM, Hitachi, S-4800). The average thickness AFM profile was calculated from over 10 different spots. The assembly ratio between GO^+ and GO^- was evaluated using a quartz crystal microbalance (QCM, Stanford Research Systems, QCM200). The analysis of the streaming ζ-potential of the $(GO^+/GO^-)_n$ multilayers was performed with a Zetasizer instrument using 1.0 M NaCl and a flat surface cell. The cross-section image of the GO multilayers was measured by advanced transmission electron microscopy (advanced TEM, Titan G2) after a focused-ion-beam sampling (FIB, Quanta 3D).

2.5. Swelling and electrochemical experiments

The dynamic response of the film thickness to different pH solutions was evaluated *via* ellipsometry in a custom-made liquid cell. The swelling experiment consists on comparing the *in-situ* thickness of the $(GO^+/GO^-)_n$ multilayers before and after exposure to pH-adjusted water. The AFM morphology of GO multilayers was measured in an *in-situ* fluid exchange cell. The electrochemical characterization was performed using a standard three-electrode cell configuration (Biologic Science Instruments, VSP). The cyclic voltammogram (CV) of ionic redox probes for the ion-permeation analysis was also based on a standard three-electrode system cell. The working electrode was the $(GO^+/GO^-)_{10}$ multilayer assembled on a fluorine doped tin oxide (FTO) substrate, which was coated with the cationic primer poly (ethyleneimine) (PEI) to promote the adhesion of the GO layers. A saturated calomel electrode (SCE) and Pt mesh were selected as reference and counter electrodes, respectively. Potassium ferricyanide and hexaaammineruthenium (III) chloride were the anionic and cationic redox probes, at an ionic concentration of 1 mM in a 0.5 M potassium chloride electrolytic solution. The potential sweep rate in CV was 50 mV/s.

3. Results and discussion

After the synthesis of the GO nanosheets (GO^-) and its subsequent functionalization with ethylenediamine to afford the positively charged GO (GO^+), the dimension and morphology were characterized by atomic force microscopy (AFM). The AFM images show the successful exfoliation of monolayered GO sheets with a lateral size from a few hundreds of nanometers to few micrometers (Fig. S1). The average thickness of the GO sheets was 0.93 ± 0.11 nm for GO^- and 1.46 ± 0.19 nm for GO^+, demonstrating the monolayered profile. The

increased thickness in GO^+ sheets indicates the successful functionalization using amine groups on the GO^- sheets. The monolayer nature of each nanosheet suggests a suitable profile for LbL assembly.

The electrostatic LbL assembly is based on the consecutive adsorption of oppositely charged polyelectrolytes. Thus, the distribution of surface charges on these 2D polyelectrolytes is an essential prerequisite to integrate both GO nanosheets in the LbL assembly. We thus examined the ζ-potential of each nanosheet under different pH conditions. The results revealed that the nanosheets had a pH-responsive charge distribution depending on the protonation/deprotonation state of the carboxylic acids and amine groups (Fig. S1). Particularly, three different pH sets were selected for the GO^+ and GO^- suspensions (pH 3/3, 7/7, and 10.5/10.5) to demonstrate how the $(GO^+/GO^-)_n$ multilayer assembly was affected by the charge distribution between components. Moreover, these pH-controlled assemblies of $(GO^+/GO^-)_n$ multilayered membrane exhibit different swelling behavior.

In the LbL assembly process, several non-covalent interactions (*e.g.*, electrostatic, hydrogen bonding and π-π stacking) induce the multilayer growth. Compared to simple polyelectrolytes assembly, it is worth noting that π-π stacking affects the multilayer assembly in these GO-based 2D polyelectrolytes. The key mechanism for the multilayer film growth is the electrostatic interaction, which leads to surface charge compensation of the adsorbed polyelectrolyte after each deposition step (Fig. 1) [33,34]. Therefore, the electrostatic interaction and the intrinsic charge balance between oppositely charged layers are the driving force of the conventional LbL assembly [35]. This intrinsic charge compensation is directly related to the ionization degree, which, in turn, controls the degree of adsorption in each cycle. The ionization degree of GO^- was also investigated *via* the relative area calculation of functional groups from the FT-IR spectra (Fig. S2). It is also important to mention that some extrinsic charge compensation occurs by the counterions introduced from the medium [36,37].

After confirming the feasibility of the electrostatic interaction between the charged GO suspensions, the sequential assembly of $(GO^+/GO^-)_n$ multilayers was investigated by UV–vis spectroscopy. As Fig. 2a shows, the absorbance of the GO multilayers gradually increased with the number of bilayers, indicating a continuous and uniform LbL assembly of the GO suspensions. The thickness variation induced by the pH conditions of GO suspension was simultaneously investigated. The ellipsometric study of the $(GO^+/GO^-)_n$ multilayers revealed remarkable differences in the average bilayer thickness depending on the pH: 3.67 nm (pH 3/3), 2.25 nm (pH 7/7), and 3.78 nm (pH 10.5/10.5) (Fig. 2b).

During film growth, the main mechanism is the charge compensation that occurs after each deposition step. In this study, the growth ratio between components (*i.e.*, GO^- and GO^+) is clearly dependent on the pH (Fig. 3a). The deposition ratio between GO^+ and GO^- in the 4 BL (*i.e.*, eight layers) assembly was 34:66 (pH 3/3), 44:56 (pH 7/7) and 78:22 (pH 10.5/10.5). This growth behavior corresponds to the weakly distributed charges in the GO^+ nanosheets against the GO^- nanosheets, which are in a highly deprotonated and ionized state in alkaline conditions. It has been reported that GO^- nanosheets have several pK_a values as they possess diverse functionalities, including sp^2-conjugated carboxylic acids, free carboxylic acids, and phenol groups [38]. Unlike GO^-, the functionality in GO^+ nanosheets is mainly the primary amine, which results in the rapid transition of charge density depending on the pH. Assuming the fully protonated GO^+ at pH 3, the ionization degree of GO^- is estimated as 3%. Conversely, when GO^- is fully ionized at pH 10.5, the ionization degree of GO^+ is merely 1%. The FT-IR spectra of the GO^- suspension further supported the variation in charge density at different pH conditions (Fig. S2). To compensate the charge balance between GO^- and GO^+ during the LbL assembly, more GO^- than GO^+ is required at pH 3/3, and the opposite occurs at pH 10.5/10.5.

Additionally, the streaming ζ-potential method was used to determine the surface charge density of the thin film membrane during the deposition of the GO layers (Fig. 3b). The LbL assembly at pH 3 was selected to highlight the inversion of surface ζ-potential during the layer deposition in agreement with the assemblies of the LbL systems. Interestingly, a non-symmetric charge reversal was observed in the deposition process from positive to negative GO layer, confirming the non-perfect direct charge compensation. Thereby, as previously hypothesized, the growth regime of the graphene film in acidic pH does not follow a perfect intrinsic charge compensation but other diffusional and dynamic compensation mechanisms may occur under this condition. Moreover, the surface charge changes were evaluated with respect to the pH for the LbL film assembled in acidic pH 3/3 conditions. The thin film potential oscillation showed the effect of the ionization of the overall film charges, demonstrating the pH-sensitive properties of the GO thin film membrane, as observed for common polyelectrolyte multilayers.

The growth mechanism of the $(GO^+/GO^-)_{10}$ multilayers were further analyzed with various microscopy techniques, including AFM, scanning electron microscopy (SEM) and cross-sectional transmission electron microscopy (TEM). As previously discussed, the pH of the GO solution influences the intrinsic properties, especially the charge density of GO nanosheets and the growth mode of $(GO^+/GO^-)_{10}$ multilayered membrane (Fig. 4). Compared to the film obtained under neutral conditions, the surface morphology of the $(GO^+/GO^-)_{10}$ multilayer films roughens in the samples assembled in both acidic and basic conditions (Fig. 4a–c).

The cross-sectional TEM allowed to obtain the thickness profiles of the $(GO^+/GO^-)_{10}$ multilayered membranes assembled at different pH (Fig. 4d–f). The *d*-spacing of each GO membrane measured from the inversed fast Fourier transformed (IFFT) histogram of the TEM corresponded to *ca.* 4.9 Å (pH 3/3), 4.0 Å (pH 7/7), and 5.3 Å (pH 10.5/10.5). It is worth noting that these *d*-spacing distances are much smaller than that of vacuum filtered GO membranes (9.0 Å), but still larger than that of graphite (3.4 Å) [39]. This intermediate *d*-spacing value implies

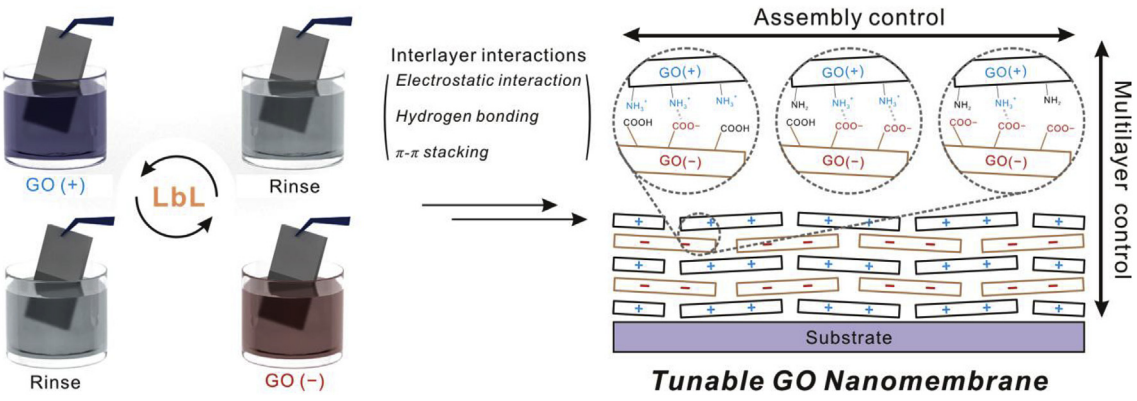

Fig. 1. Schematic illustration of layer-by-layer (LbL) assembly process of graphene oxide nanomembrane.

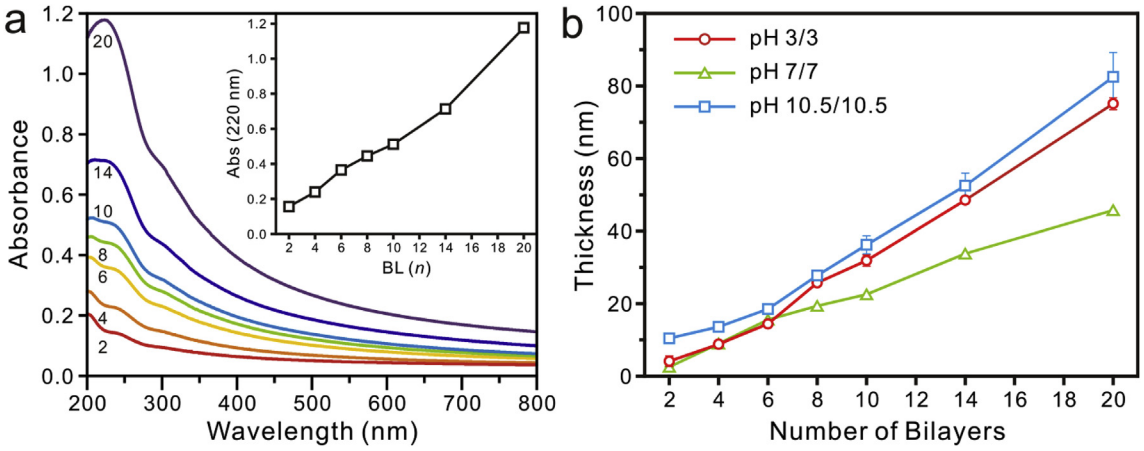

Fig. 2. (a) Representative UV–vis spectra for $(GO^+/GO^-)_n$ multilayers assembled at pH 3/3. The inset shows the peak absorbance at 220 nm as a function of the number of bilayers (BL, *n*). (b) Ellipsometric thickness profiles of the assembled $(GO^+/GO^-)_n$ multilayers with the number of bilayers. The indicated pH values represent the conditions of each solution (GO^+ and GO^-).

that the GO nanosheets are tightly holding each other based on the GO^+ and GO^- electrostatic interaction, while still maintaining proper interlayer spaces for the mass transport pathway. Such characteristics are crucial for membrane applications, particularly for gas transport through the membrane.

According to the thickness growth and roughness profiles, the film assembled in alkaline pH was the thickest and roughest, confirming the hypothesis of a random layer conformation of 2D GO polyelectrolytes. A moderate growth of multilayers in neutral pH 7/7 suggests that each GO^+ and GO^- nanosheet displays a homogenous charge distribution, which leads to strong binding between the charged, yet planar GO layers. Due to this strong binding between 2D GO-based polyelectrolytes, a dense and thin film is formed with a relatively small amount of each GO nanosheet. Meanwhile, the acidic pH 3/3 condition yields a large amount of adsorbed GO pairs with a thick film growth, originating from the charge compensation between weakly charged GO^- nanosheets and highly protonated GO^+ nanosheets.

One of the main objectives of this study is to understand the behavior of GO multilayered membranes toward swelling in water and its selective ion exchange process. GO is essentially covered with hydrophilic functional groups that results in its high water-permeability. It is widely accepted that the presence of 2D pores between the stacked GO layers allows for the diffusion of interlayer water molecules and ions [40–43]. Such process is observed when in contact with an aqueous environment and it induces the expansion in the interlayer followed by an increment in the film thickness [44].

After the characterization of the as-assembled GO multilayers, the surface morphology of the swollen GO multilayer was further explored using environmental AFM (Fig. 5). In general, the surface of the GO membrane roughened after immersion in water. It is worth noting that the film assembled in pH 10.5/10.5 displayed a significant variation in the root-mean-square roughness (R_{rms}), from 101 to 145 nm, which agrees with the previous observations. Moreover, it is interesting to observe that water swelling finished as soon as the film wets, and remained stable, without losing its integrity, for over 1 h (Fig. S3). This remarkably contrasts the previous report of Zheng et al., who observed the gradual swelling behavior of a GO membrane that was prepared *via* vacuum filtration and evaporation at 60 °C, after immersion into water over a 100 h [43]. This instant swelling behavior while retaining the integrity may be useful for several applications that require mass transport through the membrane in aqueous media, highlighting the importance of the LbL assembly technique.

This phenomenon was also quantitatively evaluated by the *in-situ* water uptake measurement using a quartz crystal microbalance with the dissipation (QCM-D) technique (Fig. 6a). Supporting the morphology changes detected under environmental AFM, the water uptake

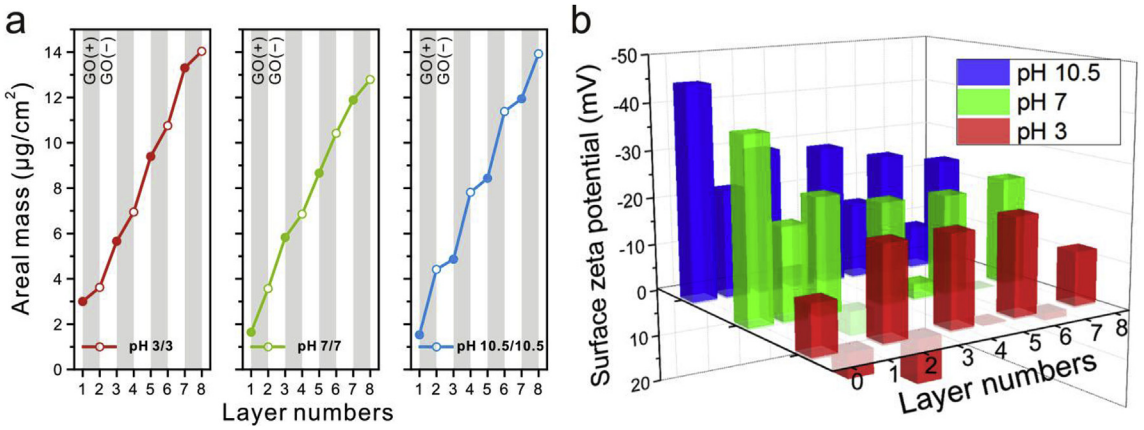

Fig. 3. (a) Growth curve of the $(GO^+/GO^-)_n$ multilayers measured with QCM under different pH conditions. Deposition of alternate GO layers is indicated with different colors (GO^+: gray, GO^-: white). (b) The surface charge variation of the $(GO^+/GO^-)_n$ multilayered membrane assembled at pH 3/3, along with the dipping in pH-adjusted solutions (pH 3, 7, and 10.5). Note that (i) the *z*-axis is in reverse order for clarity and (ii) the layer numbers are alternating single layers of GO^+ and GO^- (layer zero denotes the bare SiO_2 substrate). (For interpretation of the references to color in this figure legend, the reader is referred to the Web version of this article.)

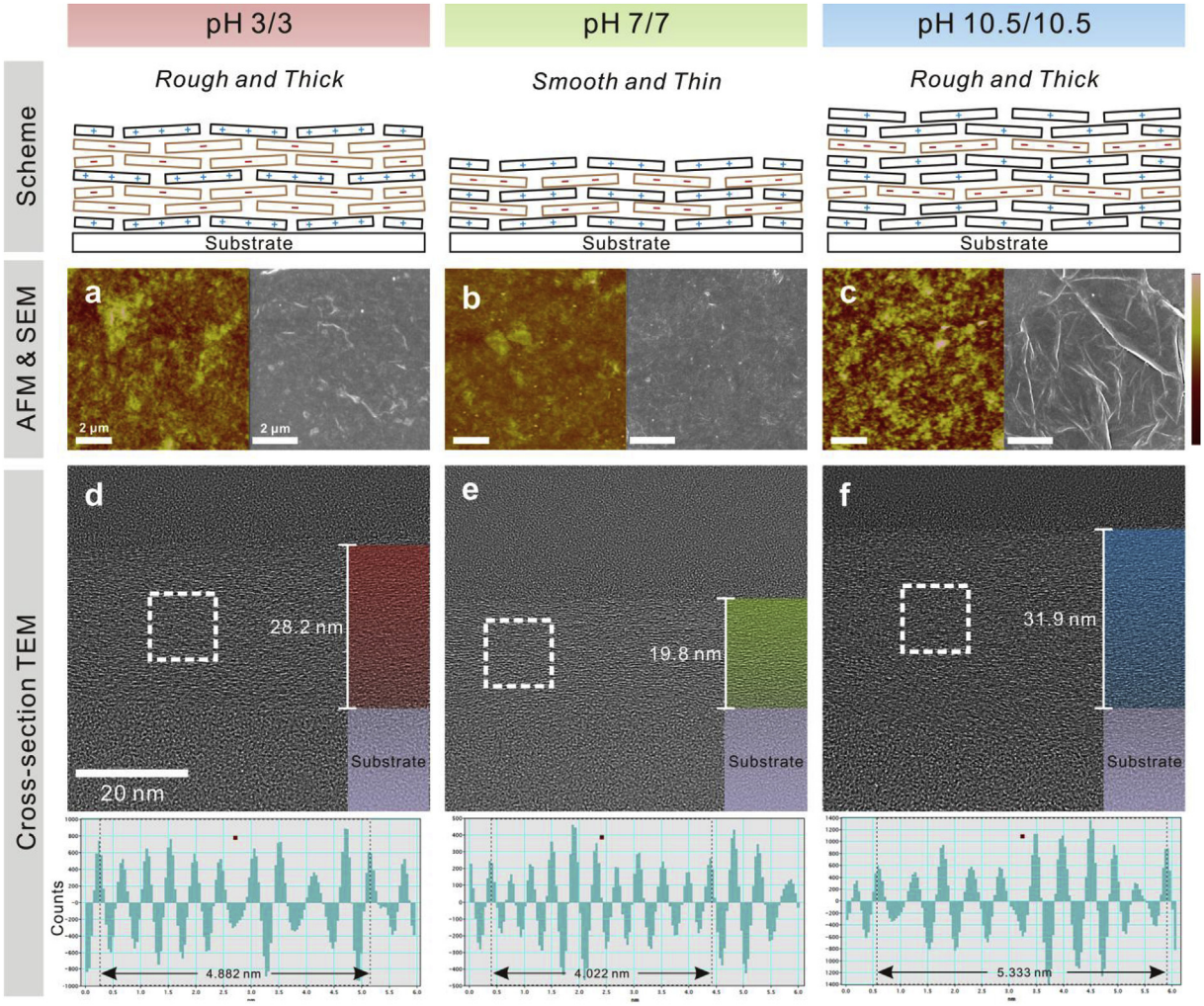

Fig. 4. Thickness and morphology variation in the $(GO^{+}/GO^{-})_{10}$ multilayer membranes assembled under different pH conditions. (a-c) Surface morphologies observed *via* AFM and SEM. (d-f) representative cross-sectional TEM images of the $(GO^{+}/GO^{-})_{10}$ multilayered membranes with the corresponding IFFT histogram of the selected area (white dashed box).

into membrane was observed in a short period (less than 30 s) in all the GO multilayered membranes. For example, the mass gain per area after the water uptake was 2.67 (pH 3/3), 1.78 (pH 7/7), and 3.28 μg/cm^2 (pH 10.5/10.5). Only a 7.44 ng/cm^2 increase was achieved for the water uptake in the blank QCM cell (without GO films assembled on the same substrate). This suggests that the assembled GO membrane is very hydrophilic and quickly attracts water molecules into the pores of the GO multilayer, while maintaining the stability of the membrane.

The swelling behavior was further explored by using acidic and alkaline media. The variation of the swollen thickness of the GO films in different pH conditions is presented in Fig. 6b for both the assembled film and exposed conditions. The film assembled in neutral conditions (pH 7/7) has the lowest swelling degree of all the pH conditions, which is in good agreement with the smooth compact structure confirmed by the previous analyses. At this pH, the charge density is similar for both building blocks (*i.e.*, similar ratio of protonated amine and deprotonated carboxylic acids on GO^{+} and GO^{-}, respectively), generating a strong electrostatic interaction between the 2D electrolytes [45]. Thus, the overall swelling degree when immersing in different pH environment is smaller due to interlayer bindings. For the assembly in alkaline conditions (pH 10.5/10.5), the swelling thickness was the highest (increased to 274%) when immersed in pH 3. The acidic media induces an instant protonation of amine groups on GO^{+}, which significantly repel each other in the pH 10.5/10.5 multilayer due to its high GO^{+} composition (*ca.* 78% from the QCM experiment). A similar swelling tendency was observed in the *in-situ* QCM experiment under identical conditions (Fig. S4). The swelling reversibility of pH 3/3 assembled $(GO^{+}/GO^{-})_{10}$ multilayer was evaluated under exposing to different pH conditions (pH 3, pH 7, and pH 10.5), which all showed a highly reversible behavior under repeated wet-and-dry cycles (Fig. S5).

Finally, to understand the ion-permeability and selectivity through GO multilayered membranes, the electrochemical behavior of $(GO^{-}/GO^{+})_{10}$ was studied by cyclic voltammetry (CV) in the presence of anionic and cationic redox probes [46]. It should be noted that the samples for electrochemical test were assembled on FTO substrate with a PEI primer layer, which reversed the assembly sequence of GO components from $(GO^{+}/GO^{-})_{n}$ to $(GO^{-}/GO^{+})_{n}$. The ion pathway in the membrane can be controlled by the assembly conditions of the GO multilayers. Compared to the bare FTO electrode, the anionic probe $K_3Fe(CN)_6$ exhibited a decrease in the redox current when using multilayered GO films, suggesting a decreased anion permeability (Fig. 7a). The redox peak was the lowest in the pH 3/3 assembled GO multilayer, supporting the assumption that a GO^{-} dominant film would inhibit the penetration of anionic species. The electrochemical measurements were performed over 25 cycles per each sample to provide a reliability and stability of GO nanomembranes (Fig. S6).

Interestingly, the cationic probe $Ru(NH_3)_6^{3+}$ showed an increased redox current when using GO multilayers regardless of the pH assembly conditions (Fig. 7b). This unexpected behavior suggests that the global charge of the multilayered GO membrane is inherently more negatively

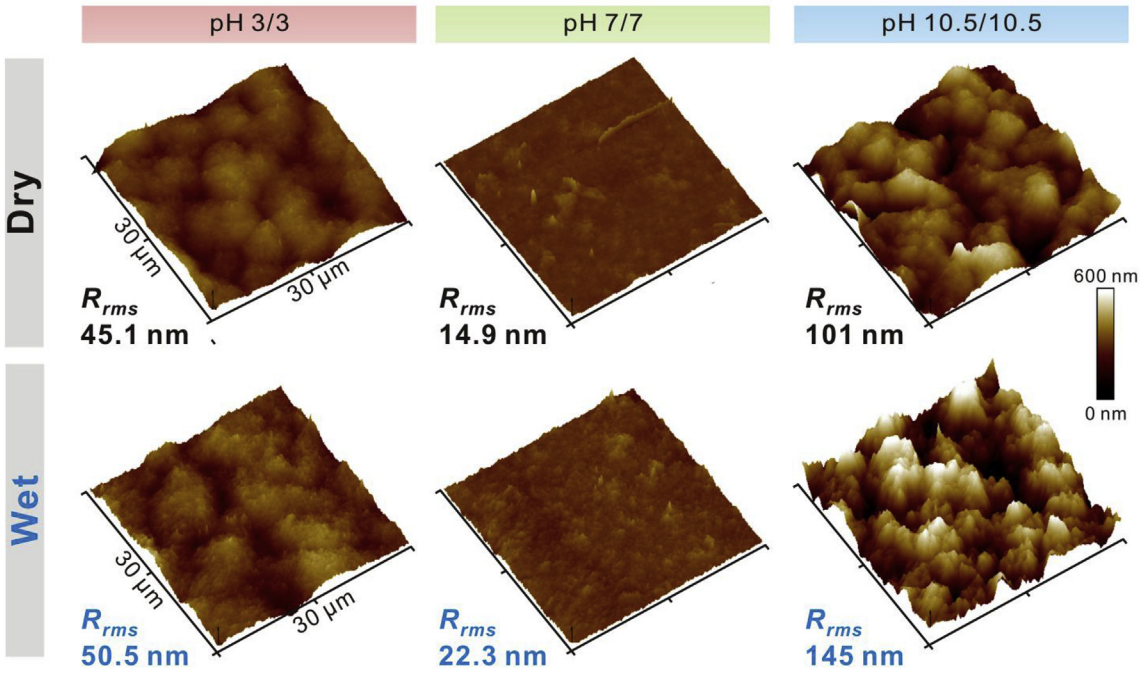

Fig. 5. Representative 3D AFM images of the $(GO^+/GO^-)_{10}$ multilayered membranes assembled on a silicon wafer, (top) before and (bottom) after swelling in DI water. R_{rms} represent the average root-mean-square roughness. (For interpretation of the references to color in this figure legend, the reader is referred to the Web version of this article.)

charged, even after the successful assembly with the GO^+ counterpart. This is also in good agreement with the streaming ζ-potential results. The retention degree of anionic species through the GO multilayered membrane was completely hindered at pH 3/3, 67.4% at pH 7/7, and 53.8% at pH 10.5/10.5. Overall, this implies that the anionic permeation through the GO membrane depends on the pH assembly conditions (*i.e.*, ratio between GO^+/GO^-), resulting in a tunable ion-permeability. The GO-based multilayered membrane allows for cationic permeation regardless of the pH conditions, while the anionic permeation depends on the assembly conditions [47]. For evaluation of the effect of the surface charges, we assembled $(GO^-/GO^+)_n$ nanomembranes of two different outermost layers, for example, 10 BL (GO^+ outermost layer) and 10.5 BL (GO^- outermost layer) assembled at the identical pH 7/7 condition. Interestingly, the surface charge of the outermost layer did not show noticeable differences in its respective electrochemical behavior (Fig. S7). We postulate that the net charge of the multilayer membrane is more critical in controlling the ion-permselective behavior than the outermost surface charge. This unique ion-permselective behavior of multilayered GO nanomembrane could be utilized in the cation exchange membranes.

4. Conclusion

We successfully obtained a GO-based multilayered membrane *via* LbL assembly of GO^+ and GO^- nanosheets. Depending on the pH assembly conditions, GO membranes with tunable thickness, roughness, charge density, and internal structures were prepared. The assembly mechanism corresponds to the charge compensation process between each GO nanosheets. The assembled GO nanomembranes were subjected to different post-assembly conditions, revealing through the membrane swelling and ion-permselective behaviors, unlike conventional GO membranes prepared by vacuum-assisted filtration. Our

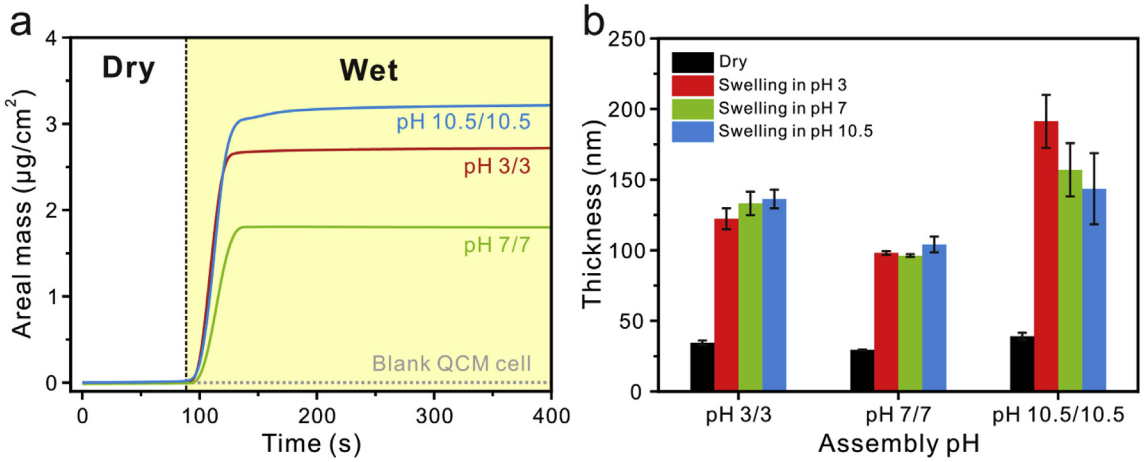

Fig. 6. (a) QCM-D based *in-situ* water uptake inside the $(GO^+/GO^-)_{10}$ multilayered membrane assembled in different pH conditions. The gray dotted line denotes the bare cell under the identical conditions as a control. (b) Ellipsometry data of water uptake inside the $(GO^+/GO^-)_{10}$ multilayered membrane with pH-adjusted water. The QCM results were extracted after 400 s of saturation. The thickness was measured in seven different spots for each sample.

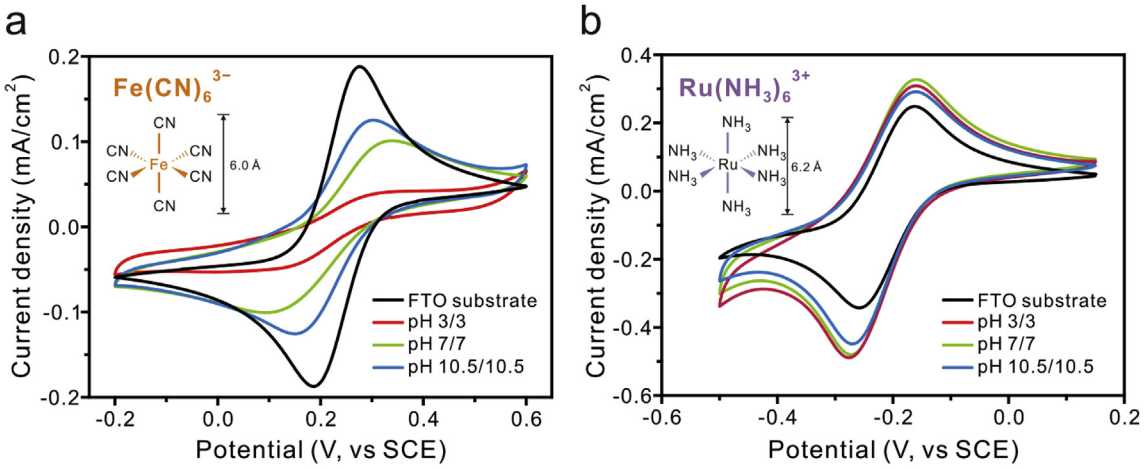

Fig. 7. Cyclic voltammograms of the $(GO^{-}/GO^{+})_{10}$ multilayered membrane assembled on a PEI-coated FTO electrode with (a) $K_3Fe(CN)_6$ and (b) $Ru(NH_3)_6Cl_3$ redox probes. Inset shows the molecular structure and size of the redox probes. Ionic concentration was 1.0 mM in a 0.50 M KCl electrolytic solution at a potential sweep rate of 50 mV/s.

discoveries on the 2D polyelectrolyte properties will provide useful guidelines to understand the physicochemical properties of graphene oxide membranes. The interesting and unique properties of the 2D polyelectrolytes evaluated in this study may be useful for a wide range of applications in materials science and membrane applications.

Acknowledgement

This work was supported by the National Research Foundation of Korea (NRF-2017M3A7B4052802) and by the Ministry of Trade, Industry and Energy, Institute for Advancement of Technology (KIAT) through the Encouragement Program for The Industries of Economic Cooperation Region (R&D, R0004883).

Appendix A. Supplementary data

Supplementary data to this article can be found online at https://doi.org/10.1016/j.memsci.2019.05.035.

Author contributions

The manuscript was written through contributions of all authors. All authors have given approval to the final version of the manuscript.

Notes

The authors declare no competing financial interest.

References

[1] A.V. Dobrynin, M. Rubinstein, Theory of polyelectrolytes in solutions and at surfaces, Prog. Polym. Sci. 30 (2005) 1049–1118, https://doi.org/10.1016/j.progpolymsci.2005.07.006.
[2] J.B. Schlenoff, H. Ly, M. Li, Charge and mass balance in polyelectrolyte multilayers, J. Am. Chem. Soc. 120 (1998) 7626–7634, https://doi.org/10.1021/ja980350+.
[3] C.J. Galvin, M.D. Dimitriou, S.K. Satija, J. Genzer, Swelling of polyelectrolyte and polyzwitterion brushes by humid vapors, J. Am. Chem. Soc. 136 (2014) 12737–12745, https://doi.org/10.1021/ja5065334.
[4] L. Zhai, F.Ç. Cebeci, R.E. Cohen, M.F. Rubner, Stable superhydrophobic coatings from polyelectrolyte multilayers, Nano Lett. 4 (2004) 1349–1353, https://doi.org/10.1021/nl049463j.
[5] P. Rivera-Gil, S. De Koker, B.G. De Geest, W.J. Parak, Intracellular processing of proteins mediated by biodegradable polyelectrolyte capsules, Nano Lett. 9 (2009) 4398–4402, https://doi.org/10.1021/nl902697j.
[6] L. Séon, P. Lavalle, P. Schaaf, F. Boulmedais, Polyelectrolyte multilayers: a versatile tool for preparing antimicrobial coatings, Langmuir 31 (2015) 12856–12872, https://doi.org/10.1021/acs.langmuir.5b02768.
[7] W. Xu, P.A. Ledin, V.V. Shevchenko, V.V. Tsukruk, Architecture, assembly, and emerging applications of branched functional polyelectrolytes and poly(ionic liquid)s, ACS Appl. Mater. Interfaces 7 (2015) 12570–12596, https://doi.org/10.1021/acsami.5b01833.
[8] K. He, H. Duan, G.Y. Chen, X. Liu, W. Yang, D. Wang, Cleaning of oil fouling with water enabled by zwitterionic polyelectrolyte coatings: overcoming the imperative challenge of oil–water separation membranes, ACS Nano 9 (2015) 9188–9198, https://doi.org/10.1021/acsnano.5b03791.
[9] A.K. Geim, K.S. Novoselov, The rise of graphene, Nat. Mater. 6 (2007) 183–191, https://doi.org/10.1038/nmat1849.
[10] K.P. Loh, Q. Bao, P.K. Ang, J. Yang, The chemistry of graphene, J. Mater. Chem. 20 (2010) 2277–2289, https://doi.org/10.1039/B920539J.
[11] D.R. Dreyer, S. Park, C.W. Bielawski, R.S. Ruoff, The chemistry of graphene oxide, Chem. Soc. Rev. 39 (2010) 228–240, https://doi.org/10.1039/B917103G.
[12] D.D. Kulkarni, I. Choi, S.S. Singamaneni, V.V. Tsukruk, Graphene Oxide−Polyelectrolyte nanomembranes, ACS Nano 4 (2010) 4667–4676, https://doi.org/10.1021/nn101204d.
[13] Q. Ji, I. Honma, S.M. Paek, M. Akada, J.P. Hill, A. Vinu, K. Ariga, Layer-by-layer films of graphene and ionic liquids for highly selective gas sensing, Angew. Chem. Int. Ed. 49 (2010) 9737–9739, https://doi.org/10.1002/anie.201004929.
[14] D.W. Lee, T.-K. Hong, D. Kang, J. Lee, M. Heo, J.Y. Kim, B.-S. Kim, H.S. Shin, Highly controllable transparent and conducting thin films using layer-by-layer assembly of oppositely charged reduced graphene oxides, J. Mater. Chem. 21 (2011) 3438–3442, https://doi.org/10.1039/c0jm02270e.
[15] J.-T. Chen, Y.-J. Fu, Q.-F. An, S.-C. Lo, S.-H. Huang, W.-S. Hung, C.-C. Hu, K.-R. Lee, J.-Y. Lai, Tuning nanostructure of graphene oxide/polyelectrolyte LbL assemblies by controlling pH of GO suspension to fabricate transparent and super gas barrier films, Nanoscale 5 (2013) 9081–9088, https://doi.org/10.1039/C3NR02845C.
[16] J. Zhu, H. Zhang, N.A. Kotov, Thermodynamic and structural insights into nanocomposites engineering by comparing two materials assembly techniques for graphene, ACS Nano 7 (2013) 4818–4829, https://doi.org/10.1021/nn400972t.
[17] K. Jo, M. Gu, B.-S. Kim, Ultrathin supercapacitor electrode based on reduced graphene oxide nanosheets assembled with photo-cross-linkable polymer: conversion of electrochemical kinetics in ultrathin films, Chem. Mater. 27 (2015) 7982–7989, https://doi.org/10.1021/acs.chemmater.5b03296.
[18] X. Zhang, H. Chen, H. Zhang, Layer-by-layer assembly: from conventional to unconventional methods, Chem. Commun. (2007) 1395–1405, https://doi.org/10.1039/B615590A.
[19] V. Gribova, R. Auzely-Velty, C. Picart, Polyelectrolyte multilayer assemblies on materials surfaces: from cell adhesion to tissue engineering, Chem. Mater. 24 (2012) 854–869, https://doi.org/10.1021/cm2032459.
[20] J.J. Richardson, J. Cui, M. Björnmalm, J.A. Braunger, H. Ejima, F. Caruso, Innovation in layer-by-layer assembly, Chem. Rev. 116 (2016) 14828–14867, https://doi.org/10.1021/acs.chemrev.6b00627.
[21] E. Ahn, B.-S. Kim, Multidimensional thin film hybrid electrodes with MoS_2 multilayer for electrocatalytic hydrogen evolution reaction, ACS Appl. Mater. Interfaces 9 (2017) 8688–8695, https://doi.org/10.1021/acsami.6b15251.
[22] P. Joo, B.J. Kim, E.K. Jeon, J.H. Cho, B.-S. Kim, Optical switching of the Dirac point in graphene multilayer field-effect transistors functionalized with spiropyran, Chem. Commun. 48 (2012) 10978–10980, https://doi.org/10.1039/C2CC35933B.
[23] H. Hwang, P. Joo, M.S. Kang, G. Ahn, J.T. Han, B.-S. Kim, J.H. Cho, Highly tunable charge transport in layer-by-layer assembled graphene transistors, ACS Nano 6 (2012) 2432–2440, https://doi.org/10.1021/nn2047197.
[24] T. Lee, S.H. Min, M. Gu, Y.K. Jung, W. Lee, J.U. Lee, D.G. Seong, B. Kim, Layer-by-Layer assembly for graphene-based multilayer nanocomposites: synthesis and applications, Chem. Mater. 27 (2015) 3785–3796, https://doi.org/10.1021/acs.chemmater.5b00491.
[25] R.R. Nair, H.A. Wu, P.N. Jayaram, I.V. Grigorieva, A.K. Geim, Unimpeded permeation of water through helium-leak-tight graphene-based membranes, Science 335 (2012) 442–444, https://doi.org/10.1126/science.1211694.

[26] R.K. Joshi, P. Carbone, F.C. Wang, V.G. Kravets, Y. Su, I. V Grigorieva, H.A. Wu, A.K. Geim, R.R. Nair, Precise and ultrafast molecular sieving through graphene oxide membranes, Science 343 (2014) 752–754, https://doi.org/10.1126/science.1245711.
[27] J.Y. Chong, B. Wang, C. Mattevi, K. Li, Dynamic microstructure of graphene oxide membranes and the permeation flux, J. Membr. Sci. 549 (2018) 385–392, https://doi.org/10.1016/j.memsci.2017.12.018.
[28] Y.-H. Xi, Z. Liu, J. Ji, Y. Wang, Y. Faraj, Y. Zhu, R. Xie, X.-J. Ju, W. Wang, X. Lu, L.-Y. Chu, Graphene-based membranes with uniform 2D nanochannels for precise sieving of mono-/multi-valent metal ions, J. Membr. Sci. 550 (2018) 208–218, https://doi.org/10.1016/j.memsci.2017.12.057.
[29] E. Yang, M.-H. Ham, H.B. Park, C.-M. Kim, J. Song, I.S. Kim, Tunable semi-permeability of graphene-based membranes by adjusting reduction degree of laminar graphene oxide layer, J. Membr. Sci. 547 (2018) 73–79, https://doi.org/10.1016/j.memsci.2017.10.039.
[30] W.S. Hummers, R.E. Offeman, Preparation of graphitic oxide, J. Am. Chem. Soc. 80 (1958), https://doi.org/10.1021/ja01539a017 1339–1339.
[31] Y. Xu, H. Bai, G. Lu, C. Li, G. Shi, Flexible graphene films via the filtration of water-soluble noncovalent functionalized graphene sheets, J. Am. Chem. Soc. 130 (2008) 5856–5857, https://doi.org/10.1021/ja800745y.
[32] E. Ahn, T. Lee, M. Gu, M. Park, S.H. Min, B.-S. Kim, Layer-by-Layer assembly for graphene-based multilayer nanocomposites: the field manual, Chem. Mater. 29 (2017) 69–79, https://doi.org/10.1021/acs.chemmater.6b02688.
[33] K. Lowack, C.A. Helm, Molecular mechanisms controlling the self-assembly process of polyelectrolyte multilayers, Macromolecules 31 (1998) 823–833, https://doi.org/10.1021/ma9614454.
[34] J. Borges, J.F. Mano, Molecular interactions driving the layer-by-layer assembly of multilayers, Chem. Rev. 114 (2014) 8883–8942, https://doi.org/10.1021/cr400531v.
[35] J.B. Schlenoff, S.T. Dubas, Mechanism of polyelectrolyte multilayer Growth: charge overcompensation and distribution, Macromolecules 34 (2001) 592–598, https://doi.org/10.1021/ma0003093.
[36] R.A. Ghostine, M.Z. Markarian, J.B. Schlenoff, Asymmetric growth in polyelectrolyte multilayers, J. Am. Chem. Soc. 135 (2013) 7636–7646, https://doi.org/10.1021/ja401318m.
[37] D. Kim, S. Lee, Y. Ko, C.H. Kwon, J. Cho, Layer-by-layer assembly-induced triboelectric nanogenerators with high and stable electric outputs in humid environments, Nanomater. Energy 44 (2018) 228–239, https://doi.org/10.1016/j.nanoen.2017.12.001.
[38] B. Konkena, S. Vasudevan, Understanding aqueous dispersibility of graphene oxide and reduced graphene oxide through pKa measurements, J. Phys. Chem. Lett. 3 (2012) 867–872, https://doi.org/10.1021/jz300236w.
[39] D.W. Kim, J. Choi, D. Kim, H.-T. Jung, Enhanced water permeation based on nanoporous multilayer graphene membranes: the role of pore size and density, J. Mater. Chem. A. 4 (2016) 17773–17781, https://doi.org/10.1039/C6TA06381K.
[40] P. Sun, M. Zhu, K. Wang, M. Zhong, J. Wei, D. Wu, Z. Xu, H. Zhu, Selective ion penetration of graphene oxide membranes, ACS Nano 7 (2013) 428–437, https://doi.org/10.1021/nn304471w.
[41] R. Zahn, K.R. Bickel, T. Zambelli, J. Reichenbach, F.M. Kuhn, J. Vörös, R. Schuster, The entropy of water in swelling PGA/PAH polyelectrolyte multilayers, Soft Matter 10 (2014) 688–693, https://doi.org/10.1039/C3SM52489B.
[42] A. Klechikov, J. Yu, D. Thomas, T. Sharifi, A.V. Talyzin, Structure of graphene oxide membranes in solvents and solutions, Nanoscale 7 (2015) 15374–15384, https://doi.org/10.1039/C5NR04096E.
[43] S. Zheng, Q. Tu, J.J. Urban, S. Li, B. Mi, Swelling of graphene oxide membranes in aqueous solution: characterization of interlayer spacing and insight into water transport mechanisms, ACS Nano 11 (2017) 6440–6450, https://doi.org/10.1021/acsnano.7b02999.
[44] T. Daio, T. Bayer, T. Ikuta, T. Nishiyama, K. Takahashi, Y. Takata, K. Sasaki, S. Matthew Lyth, In-situ ESEM and EELS observation of water uptake and ice formation in multilayer graphene oxide, Sci. Rep. 5 (2015) 11807, https://doi.org/10.1038/srep11807.
[45] J.M. Silva, S.G. Caridade, R.R. Costa, N.M. Alves, T. Groth, C. Picart, R.L. Reis, J.F. Mano, pH responsiveness of multilayered films and membranes made of polysaccharides, Langmuir 31 (2015) 11318–11328, https://doi.org/10.1021/acs.langmuir.5b02478.
[46] M.-K. Park, S. Deng, R.C. Advincula, pH-sensitive bipolar ion-permselective ultrathin films, J. Am. Chem. Soc. 126 (2004) 13723–13731, https://doi.org/10.1021/ja0484707.
[47] M. Gu, J. Lee, Y. Kim, J.S. Kim, B.Y. Jang, K.T. Lee, B.-S. Kim, Inhibiting the shuttle effect in lithium-sulfur batteries using a layer-by-layer assembled ion-permselective separator, RSC Adv. 4 (2014) 46940–46946, https://doi.org/10.1039/c4ra09718a.